GLOBAL CARBON CYCLE

Abrupt CO_2 release to the atmosphere under glacial and early interglacial climate conditions

C. Nehrbass-Ahles[1,2,3]*, J. Shin[4], J. Schmitt[1,2], B. Bereiter[1,2,5], F. Joos[1,2], A. Schilt[1,2], L. Schmidely[1,2], L. Silva[1,2], G. Teste[4], R. Grilli[4], J. Chappellaz[4], D. Hodell[3], H. Fischer[1,2], T. F. Stocker[1,2]

Pulse-like carbon dioxide release to the atmosphere on centennial time scales has only been identified for the most recent glacial and deglacial periods and is thought to be absent during warmer climate conditions. Here, we present a high-resolution carbon dioxide record from 330,000 to 450,000 years before present, revealing pronounced carbon dioxide jumps (CDJ) under cold and warm climate conditions. CDJ come in two varieties that we attribute to invigoration or weakening of the Atlantic meridional overturning circulation (AMOC) and associated northward and southward shifts of the intertropical convergence zone, respectively. We find that CDJ are pervasive features of the carbon cycle that can occur during interglacial climate conditions if land ice masses are sufficiently extended to be able to disturb the AMOC by freshwater input.

Analyses of Antarctic ice cores have demonstrated that atmospheric CO_2 has been a major driver of Earth's climate on orbital to millennial time scales (*1*–*3*). However, evidence of submillennial-scale CO_2 variability is only available for the past ~60 thousand years (ka), that is, not beyond the last glacial period (*4*–*6*). Climate-carbon cycle perturbations during previous interglacial periods serve as first-order templates for the natural response of Earth's climate system to warmer climatic background conditions (*7*), but the use of CO_2 records to decipher submillennial-scale variations has thus far been hampered by insufficient temporal resolution of existing ice core records.

Previous research identified two principal modes of CO_2 variability on millennial to centennial time scales: (i) millennial-scale carbon dioxide maxima (CDM) frequently occurring during the last glacial period (*4*, *5*, *8*) and (ii) centennial-scale carbon dioxide jumps (CDJ) caused by pulse-like CO_2 releases to the atmosphere, most prominently occurring during the last deglaciation (*6*, *9*).

CDM are characterized by a triangular shape of evolving CO_2 changes. They closely covary with Antarctic temperature proxy records on millennial time scales, as evidenced by the Antarctic isotope maxima (*4*, *8*, *10*). During cold periods (stadials) in the Northern Hemisphere (NH), CO_2 is observed to increase gradually and in parallel to the bipolar seesaw response in Antarctic temperature (*11*) at typical rates of ~1 part per million (ppm) per century (*4*, *8*). CDM reach amplitudes of up to 30 ppm before their trends are reversed in connection with a sudden strengthening of the Atlantic meridional overturning circulation (AMOC) linking the onset of Dansgaard-Oeschger (DO) events (i.e., abrupt warming over Greenland) and the start of slow cooling in the Southern Ocean (SO) region (*4*, *8*, *11*).

In contrast, abrupt CDJ do not directly correspond to variations in Antarctic temperature but are associated with either DO events or Heinrich stadials (HS) in the NH (*6*, *12*, *13*). The latter are characterized by extended cold periods in the NH associated with a weakened AMOC (*14*–*16*). The few CDJ identified so far are superimposed on gradually increasing millennial CO_2 trends connected to CDM or glacial terminations and lead to a sudden 10 to 15 ppm CO_2 rise within less than ~250 years at rates of ~10 ppm per century, about 10 times faster than CDM. As of yet, CDJ have only been identified during the most recent deglaciation (Termination I) (*6*, *9*) and for HS 4 (*12*, *13*), occurring at 39.5 ka BP (thousand years before present, with the present defined as 1950 CE). CDJ are synchronous with either major methane (CH_4) rises linked to DO events or small CH_4 peaks associated with HS, suggesting a link with sudden AMOC changes and poleward shifts of the intertropical convergence zone (ITCZ) (*6*, *17*, *18*). Here, we address whether CDJ also occur during glacial growth phases and interglacial climate conditions and therefore whether they are a pervasive feature of the past carbon cycle.

Centennial- to millennial-scale CO_2 variability between ~150 and 400 ka BP could not be explored because of insufficient measurement precision and low temporal resolution of the existing CO_2 record for this period (*1*). Here, we investigate the older part of this interval by presenting a high-resolution record of CO_2 mole fractions covering a full glacial-interglacial cycle from 330 to 450 ka BP [i.e., marine isotope stage (MIS) 9e to MIS 12a (*19*)], measured on samples from the European Project for Ice Coring in Antarctica (EPICA) Dome C (EDC) ice core using an improved dry-extraction technique (*20*). In comparison to earlier data (*1*, *2*), we enhance the precision by a factor of three (now ~1 ppm) and increase temporal resolution between four- and sixfold (now ~300 years on average).

Additionally, we improve the resolution of the existing EDC CH_4 record (*21*) to an average of ~250 years at periods of abrupt changes (*20*). This improvement permits a direct comparison of the CH_4 imprint of fast climate changes in the NH with the Southern Hemisphere bipolar seesaw response in Antarctic temperature and atmospheric CO_2 (*4*, *8*). We combine our ice core data with new records of benthic $\delta^{13}C$ and $\delta^{18}O$ of *Cibicidoides wuellerstorfi* (*22*) and planktic $\delta^{18}O$ of *Globigerina bulloides* (*23*). These stable isotope data are measured on marine sediment core samples from the International Ocean Discovery Program (IODP) site U1385 located on the Iberian margin off the coast of Portugal at a water depth of ~2600 m below sea level (*20*). A temporal resolution of ~150 years on average enables us to directly compare our ice core data with this independent paleoclimatic archive of hydrological change in the North Atlantic (NA).

On orbital time scales, our CO_2 record reveals generally high CO_2 levels persisting above 260 ppm (*24*) over ~35 ka during the exceptionally long interglacial period MIS 11c to 11e, from 427 to 393 ka BP (Fig. 1B), extending over more than one precessional cycle (*25*). The minimum CO_2 value of 187.6 ± 1.0 ppm is reached at 358 ka BP, coinciding with the lowest sea surface temperature (SST) (Fig. 2, D, G, and H) (*26*). However, the onset of the deglacial CO_2 rise toward MIS 9e (Termination IV) only takes place ~13.5 ka later, at 344.5 ka BP. The end of this deglacial CO_2 increase (~335 ka BP) is marked by a peak CO_2 value of 300.4 ± 1.0 ppm, representing the highest natural CO_2 mole fraction derived from Antarctic ice cores over the past 800 ka. We identify, superimposed on this orbital trend, different types of millennial- to centennial-scale CO_2 variability, occurring most frequently during, but not limited to, the glacial growth phase.

On millennial time scales, the CO_2 record mirrors the variability in the EDC temperature proxy (Figs. 1A and 2A) (*10*) and dust flux records (Fig. 2B) (*27*), a feature previously observed over the past 800 ka in lower-resolution CO_2 data (*2*, *3*). Our new benthic $\delta^{18}O$ record from IODP site U1385 follows the same pattern (Fig. 2C), indicating the influence of southern-sourced deep water, as first noted for the last

[1]Climate and Environmental Physics, Physics Institute, University of Bern, Bern, Switzerland. [2]Oeschger Centre for Climate Change Research, University of Bern, Bern, Switzerland. [3]Godwin Laboratory for Palaeoclimate Research, Department of Earth Sciences, University of Cambridge, Cambridge, UK. [4]Institute of Environmental Geosciences (IGE), Grenoble INP, IRD, CNRS, Université Grenoble Alpes, Grenoble, France. [5]Laboratory for Air Pollution/ Environmental Technology, Empa–Swiss Federal Laboratories for Materials Science and Technology, Dübendorf, Switzerland.
*Corresponding author. Email: cn425@cam.ac.uk

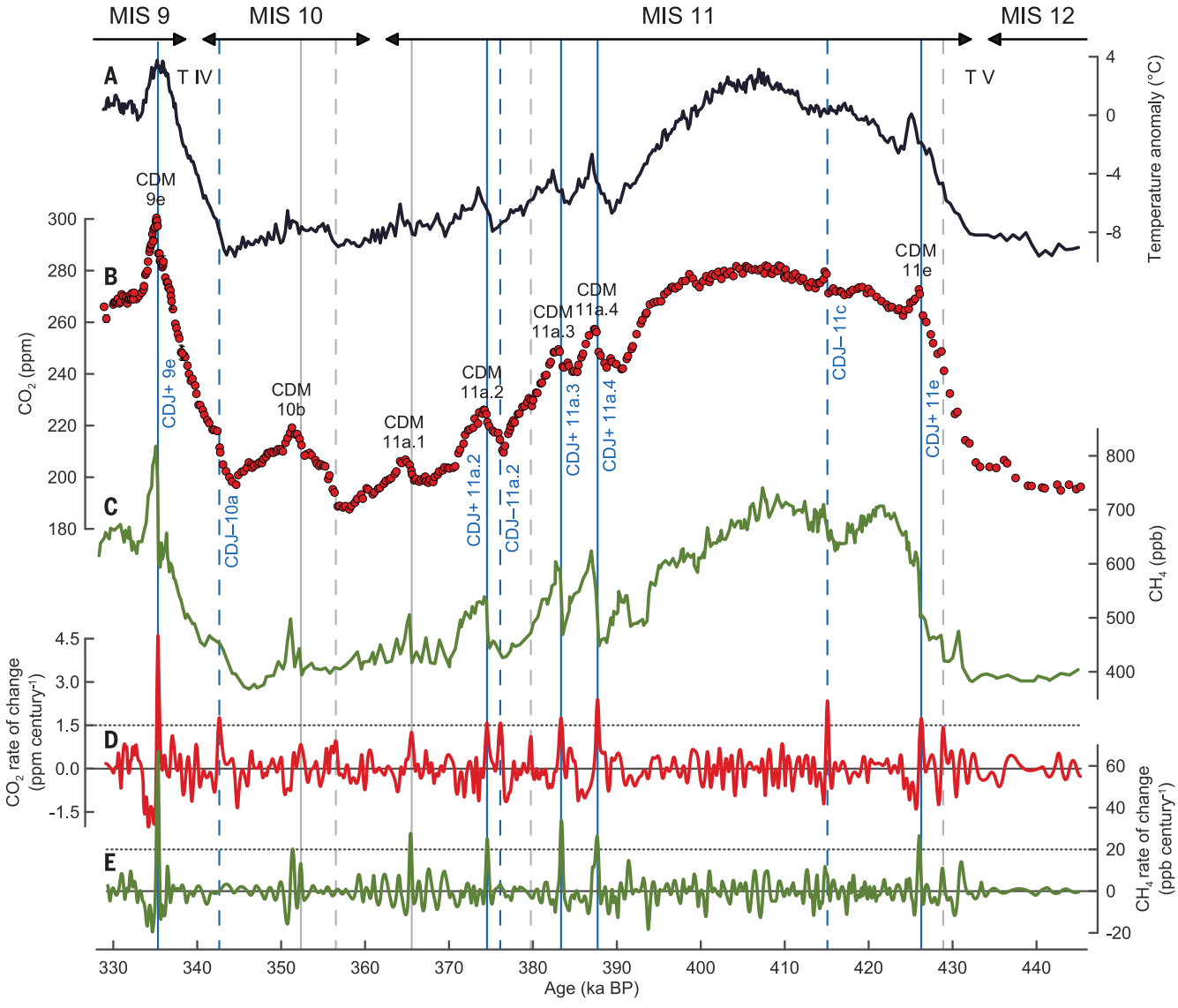

Fig. 1. High-resolution CO_2 and improved CH_4 records compared with Antarctic temperature during MIS 9e to 12a. (**A**) Antarctic temperature anomalies (*10*). (**B**) CO_2 record (this study). (**C**) CH_4 compilation (this study) (*20*). (**D**) Rate of change of CO_2 in the ice core record derived from a smoothed version of (B) (*20*). (**E**) Rate of change of CH_4 in the ice core record derived from a smoothed version of (C) (*20*). All data are based on measurements of EDC ice core samples and are plotted on the Antarctic Ice Core Chronology 2012 (AICC2012) age scale (*34*). Identified CDM and CDJ are labeled according to the MIS assignment in (*19*). Distinct CDJ in the CO_2 record are indicated with blue vertical lines, positioned at the peaks in (D) exceeding a threshold value of 1.5 ppm per century (*20*). CDJ+ (solid blue lines) coincide with major CH_4 rises greater than 50 ppb at growth rates greater than 20 ppb per century (E), whereas CDJ– (dashed blue lines) do not. Further potential events with positive rates below 1.5 ppm per century (D) are indicated with gray vertical lines but not labeled. T IV, Termination IV; T V, Termination V.

glacial period (MIS 3) (*28*). Our results demonstrate that this correlation also applies to MIS 10a to 11a, thereby emphasizing the key role of SO processes in the bipolar seesaw (*4*, *11*) and associated global-scale climate regime shifts in shaping atmospheric CO_2 on millennial time scales. We identify a total of seven CDM events (Fig. 1B). The two youngest events (CDM 9e and 10b) were reported previously (*1*), but the oldest five (CDM 11a.1, 11a.2, 11a.3, 11a.4, and 11e) were not. Furthermore, our record shows that the covariation of CO_2 and the Antarctic temperature proxy (*10*) also holds for the extended interglacial period MIS 11c (Fig. 1, A and B), where both Antarctic temperatures and CO_2 gradually increase along with the summer insolation at 65°N (*25*). The time at which CO_2 and Antarctic temperature cease to covary in our record is at the end of MIS 11c, when Antarctic temperature leads the CO_2 decrease by several thousand years, similar to what is observed for the glacial inception after the penultimate interglacial (*29*).

On the centennial time scale, we detect eight CDJ occurring under very different climate boundary conditions (Fig. 1B). They are marked by centennial-scale peaks in the rate of change of CO_2 exceeding a threshold of 1.5 ppm per century in the ice core record (Fig. 1D) (*20*). The close correlation of millennial-scale CO_2 variability with Antarctic temperature (Fig. 1A) does not hold for CDJ (Fig. 3A and fig. S1A). While all CDJ lead to an abrupt rise in CO_2 of ~10 ppm (table S1), their underlying causes may differ (*13*, *30*). We distinguish two varieties of CDJ on the basis of the presence or absence of a major simultaneous CH_4 rise at the same depth level of the ice core (*20*).

The first variety of CDJ is synchronous with rapid rises in the CH_4 record greater than

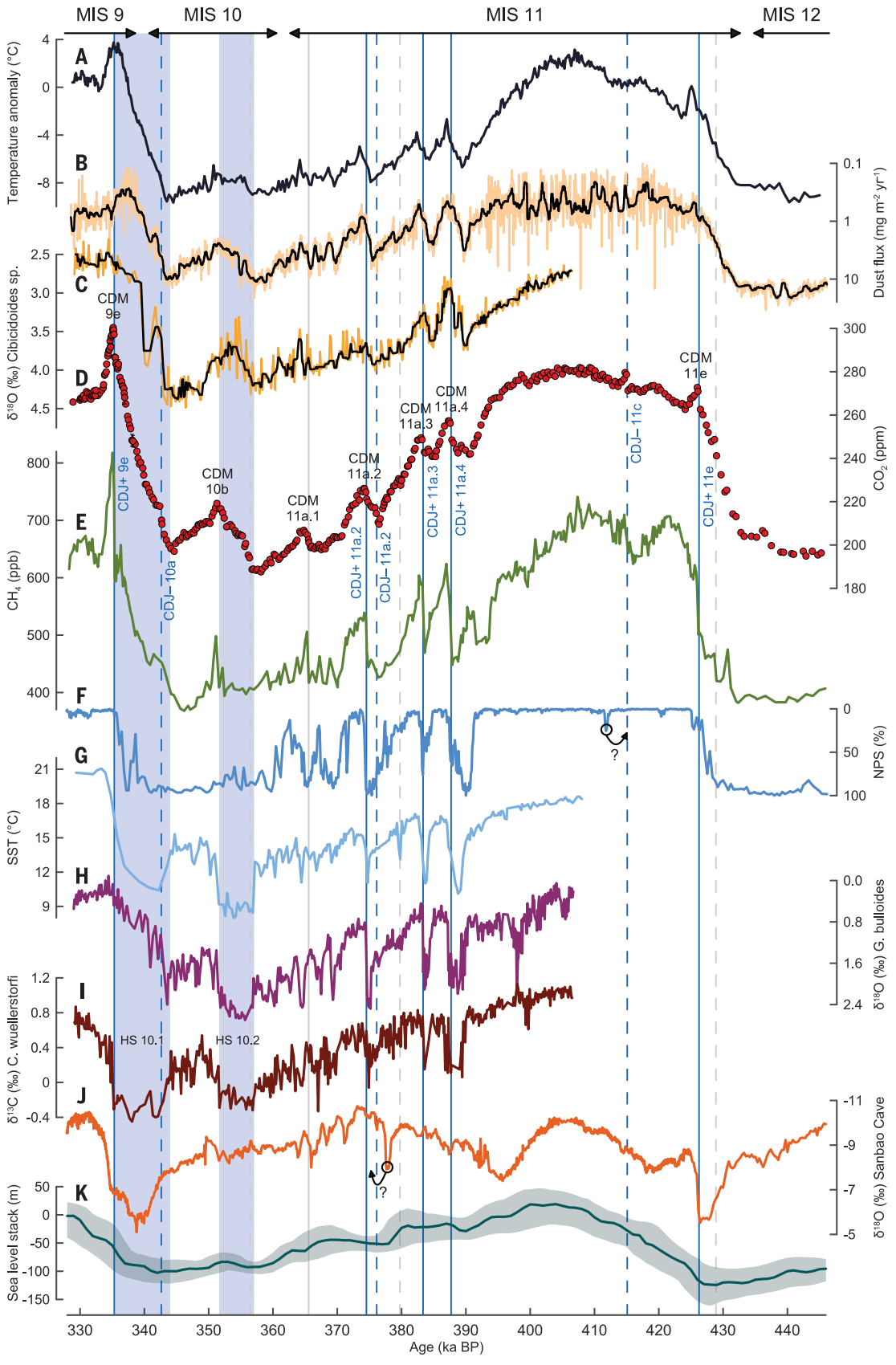

Fig. 2. Comparison of high-resolution CO_2 and improved CH_4 records with marine sediment and speleothem data covering MIS 9e to 12a. (**A**) EDC temperature anomalies (*10*). (**B**) EDC dust flux (*27*), including an ~500-year running median. (**C**) Benthic $\delta^{18}O$ *C. wuellerstorfi* from IODP site U1385 on the Iberian margin (this study), including an ~500-year running median. ‰, per mil. (**D**) EDC CO_2 record (this study). (**E**) EDC CH_4 compilation (this study) (*20*). (**F**) Relative proportion of the polar planktic foraminifera *Neogloboquadrina pachyderma* (NPS) from ODP site 983 (*38*). (**G**) $U^{K'}_{37}$-based SST from IODP site U1385 (*26*). (**H**) Planktic $\delta^{18}O$ *G. bulloides* from IODP site U1385 (this study). (**I**) Benthic $\delta^{13}C$ *C. wuellerstorfi* from IODP site U1385 (this study). (**J**) $\delta^{18}O$ Sanbao Cave record in Hubei, China (*35*). (**K**) Global sea level stack (probability maximum) including 95% probability intervals (*37*). All records are given on the AICC2012 age scale (*34*) or are transferred to AICC2012 (*20*), with the exception of (J) and (K). Arrows in (F) and (J) highlight potential age-scale inconsistencies. Labeling and vertical line styles are identical to those in Fig. 1. Vertical blue bands indicate HS 10.1 and HS 10.2 (see text for details).

50 parts per billion (ppb) (Figs. 1C and 3C) and growth rates exceeding 20 ppb per century, as recorded in the EDC ice core (Figs. 1E and 3E). We dub these pulse-like CO_2 release events CDJ+. Using this definition, we identify five CDJ+ (9e, 11a.2, 11a.3, 11a.4, and 11e) (Fig. 1B). The major CH_4 rises associated with CDJ+ indicate abrupt DO-like warming in the NH directly linked to AMOC invigorations (*6*, *17*). Direct evidence for such AMOC strengthening comes from associated abrupt rises in SST in the NH (Fig. 2, F to H) and increases of benthic $\delta^{13}C$ values (Fig. 2I), indicative of the inflow of NA deep-water masses at IODP site U1385. These findings are consistent with the two previously identified CDJ+ events during the last deglaciation, at the onsets of the Bølling-Allerød and Preboral periods (*6*, *9*).

The most pronounced CDJ+ (CDJ+ 9e) takes place during early interglacial conditions, when CO_2 values are already above 285 ppm, a level that is higher than typical peak-CO_2 mole fractions during interglacial conditions over the past 800 ka (*3*). The time resolution for CDJ+ 9e is better than 90 years and shows an exceptionally fast CO_2 increase of ~10 ppm per century, as measured on the two neighboring ice samples (Fig. 3B). Accounting for the smoothing of atmospheric signals by the bubble enclosure process, we estimate an original rate of atmospheric CO_2 increase of 26.2 ± 17.6 ppm per century (Fig. 3B and table S1) (*20*), which provides a benchmark for the possible range and speed of positive carbon cycle feedbacks connected to AMOC variations during the deglaciation. This rate exceeds previous estimates of maximum preindustrial atmospheric increase rates (*31*) by a factor of seven but is still a factor of nine lower than recent anthropogenic growth rates over the past decade (*32*). The CO_2 decrease after CDJ+ 9e shows that natural processes during interglacial conditions allowed for a sustained CO_2 removal from the atmosphere estimated at ~2 ppm per century for ~2 ka (Figs. 1B and 3B).

The second variety of CDJ occurs independently from major responses in the EDC CH_4 record (Fig. 1, C and E) (see supplementary text section of the supplementary materials) and is dubbed CDJ–. We identify two CDJ– (10a and 11a.2), which share similar characteristics with the two CDJ– events associated with HS 1 during the last deglaciation (~16 ka BP) and HS 4 (*6*, *12*, *13*). We speculate that CDJ– can be attributed to carbon cycle processes caused by AMOC weakening. Although direct AMOC records do not yet exist for MIS 9e to 12a, abrupt decreases of benthic $\delta^{13}C$ indicate intrusions of Antarctic bottom water masses at IODP site U1385 (Fig. 2I) likely due to AMOC weakening, similar to what occurred during HS in the last glacial period (*14*, *15*). Note that major HS (HS 10.1 and 10.2) are identified in Fig. 2 by the drop in alkenone saturation index ($U^{K'}_{37}$)–based SST (Fig. 2G) and the decrease in benthic $\delta^{13}C$ (Fig. 2I) indicative of a reduced state of the AMOC. Whereas CDJ– 10a is likely related to carbon cycle responses to an AMOC slowdown caused by massive ice discharge during HS 10.1 (Fig. 2I), there exists only ambiguous evidence for CDJ– 11a.2 being associated with freshwater forcing. Low CH_4 levels (Fig. 2E) and cold SST in the NA (Fig. 2F) indicate stadial conditions in the NH associated with CDJ– 11a.2. Given the relative age uncertainties between our ice core and independently dated records (*33*, *34*), the $\delta^{18}O$ calcite record from Sanbao Cave (Fig. 2J) (*35*) indicates a major shift of the ITCZ that may be associated with CDJ– 11a.2 (*18*, *36*).

Most notably, the new CO_2 record reveals the clearly distinguishable CDJ 11c (12.9 ± 2.7 ppm increase within 191 ± 123 years) (Fig.

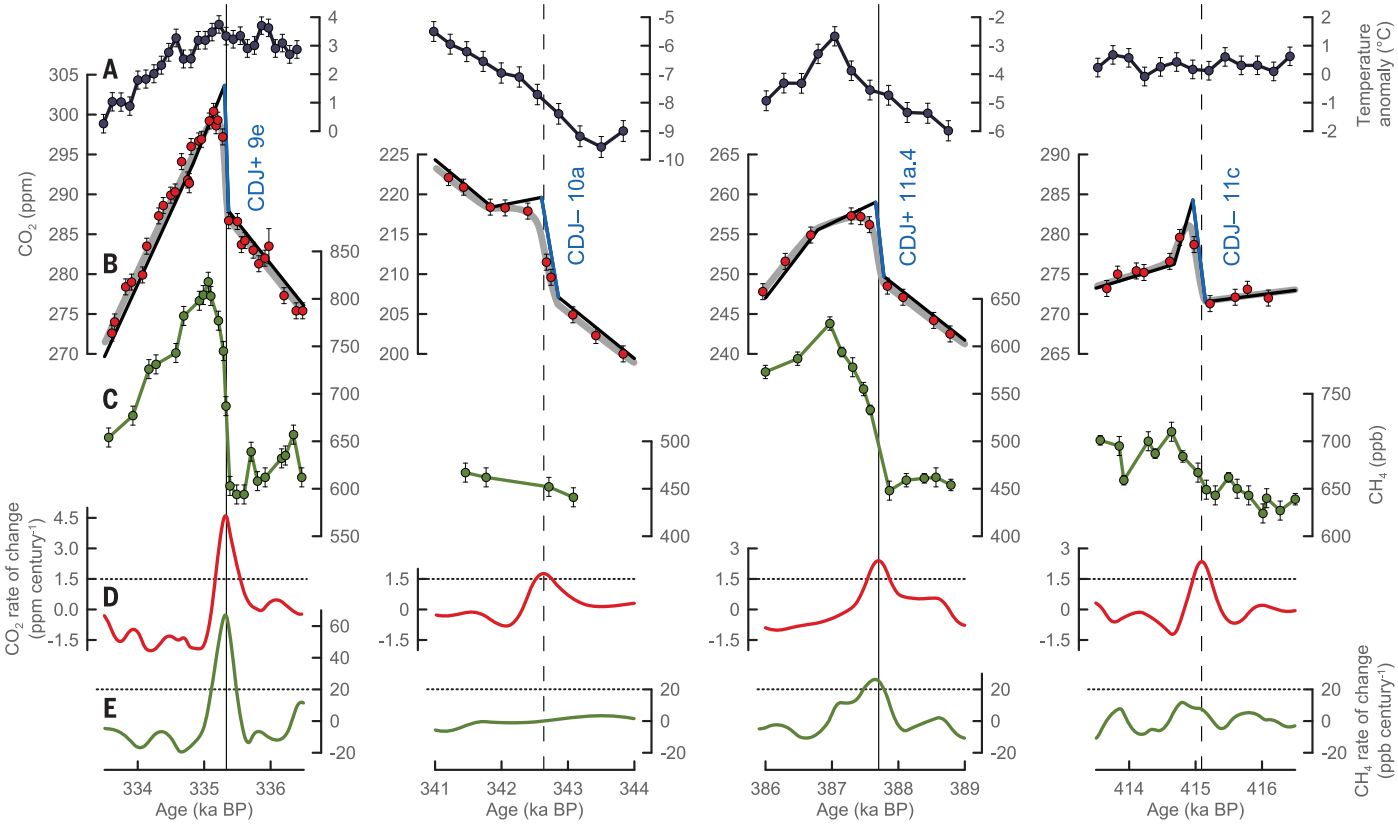

Fig. 3. Detailed view of the two varieties of CDJ. (**A** to **E**) Identical to Fig. 1. The black linear segments in (B) indicate first-order approximations of the atmospheric CO_2 evolution. The blue segment highlights the actual CDJ event. These approximations for the atmospheric trajectories are optimized so that the CO_2 curve after smoothing by the bubble enclosure process (gray lines) fits the ice core data (red dots) best. The firn smoothing is realized by applying improved gas enclosure characteristics for the EDC ice core (*20*). See table S1 for details. All remaining CDJ are shown in fig. S1.

3B and table S1) at 415 ka BP, occurring ~10 ka into interglacial temperature conditions at Dome C, but still at a time of considerable sea level rise (Fig. 2K) (*37*). A hiatus in the section older than 407 ka BP at IODP site U1385 obscures potential signals related to this event (*20*). A distinct peak found in a proxy for SST conditions at 412 ka BP (Fig. 2F) (*38*) is indicative of hydrographic disturbance in the NA. A possible perturbation of the AMOC at the same time (*39*) may be connected to this event, both of which may be attributed to a major freshwater forcing at the time of near-deglaciation of the southern Greenland Ice Sheet in the early part of MIS 11c (*40*). Another recent study suggests a major ice sheet discharge event into the SO that might also coincide with this CDJ at 415 ka BP (*41*), but dating uncertainties do not permit an unambiguous attribution. While there is limited evidence supporting an AMOC perturbation around 415 ka BP, it remains unclear whether CDJ 11c is associated with an AMOC weakening or strengthening. Given the lack of a major CH_4 rise in our record (Fig. 3, C and E), we classify this event as CDJ– (CDJ– 11c); however, it could mechanistically also be CDJ+, with an atypical CH_4 response caused by already warm climate conditions in the NH.

Invigorations of the AMOC during DO events lead to abrupt increases in cross-equatorial heat transport to the NH (*15*, *42*), which may be a necessary (yet insufficient) condition for the occurrence of CDJ+ events (*6*, *43*). As a direct consequence of this energy imbalance, the ITCZ shifts northward and promotes a poleward shift and intensification of westerlies in the NH (*18*, *42*). Driven by this shift in the ITCZ, new tropical wetlands are formed in the NH, which leads to an extended increase in CH_4 production (*17*, *18*).

Conversely, we presume that CDJ– are associated with a weakening of the AMOC, causing a southward shift of the ITCZ, which promotes the formation of wetlands in the SH. The latter results in an initial overshoot in the CH_4 production that coincides with CDJ– during HS 1 and HS 4 (*18*). These small, short-lived CH_4 peaks of amplitudes smaller than ~50 ppb are distinct from major CH_4 rises associated with CDJ+; however, both CH_4 responses proceed at comparable growth rates. The absence of any short-lived CH_4 peaks related to CDJ– in our record (Fig. 3C and fig. S1C), similar to those found for HS 1 and HS 4 (*18*), can be explained by a combination of relatively low sample resolution and the bubble enclosure process that smooths the EDC gas record. The latter results in the obliteration of any potential CH_4 peaks smaller than ~50 ppb lasting for less than 200 years (see supplementary text). Accordingly, we use the absence of a major CH_4 rise as a criterion to distinguish CDJ– from CDJ+. Whereas the climate conditions for CDJ+ are characteristic for DO events in the NH, CDJ– appear to be connected with major freshwater forcing and stadial conditions in the NH (*6*, *13*, *18*).

The strong correspondence of the CO_2 record with Antarctic temperature and benthic $\delta^{18}O$ at the Iberian margin on the millennial time scale (Fig. 2, A, C, and D) suggests a causal link of CDM formation with SO processes (*8*). Proposed CDM-generating mechanisms include perturbations in the carbon cycle owing to changes in deep SO ventilation related to changes in stratification, buoyancy forcing, and Southern Hemisphere westerlies (*44*, *45*); variations of the southern sea ice edge (*46*); and efficiency of the biological pump caused by either changes in the magnitude of dust-induced iron fertilization (*44*) or mode changes in the AMOC (*47*).

In contrast, the underlying CO_2 release mechanisms for the CDJ are poorly understood. Suggested marine mechanisms include outgassing due to increasing SST (*30*), rapid ventilation of accumulated respired carbon from intermediate-depth Atlantic (*43*, *48*), or SO deep-water masses (*49*, *50*). Despite the coherence of CDJ with AMOC changes and associated deep-water reorganizations in the NA (Fig. 2I) (*6*, *43*), the carbon source for CDJ may not necessarily originate from the ocean. Proposed terrestrial sources include permafrost thawing in the NH (*51*), drought-induced biomass decomposition (*6*, *30*), and changes in precipitation and vegetation distribution connected to ITCZ shifts (*18*, *36*). To explain a 10-ppm CDJ in the atmosphere caused by carbon release from the land biosphere, ~80 Pg of carbon are needed (*52*). For most of these processes, a shift of the position of the ITCZ and resulting changes in the mid- to high-latitude westerly winds (*53*) are necessary to couple the cross-equatorial heat transport in the NA to the global carbon cycle (*11*, *42*).

Our CO_2 record from the EDC ice core provides evidence for centennial-scale CDJ during glacial, deglacial, and early interglacial conditions. The CDJ identified here suggest fast, pulse-like CO_2 releases to the atmosphere during MIS 9e to 12a that are likely related to abrupt changes in AMOC (Fig. 2I) and shifts in the position of the ITCZ (Fig. 2E). Our data imply that CDJ are a pervasive feature of the natural carbon cycle that may go undetected in CO_2 records of insufficient temporal resolution and precision. We stress that such CDJ also occur during interglacial temperature conditions, as long as freshwater discharge from remnant ice sheets persists and is able to disturb ocean circulation. Anthropogenic warming and the committed ice sheet melting and associated sea level rise over the coming millennia (*54*) constitute new drivers that might trigger ocean circulation changes, and hence, pulse-like CO_2 releases such as those detected in our record during an earlier interglacial period when AMOC was perturbed.

REFERENCES AND NOTES

1. J. R. Petit *et al.*, *Nature* **399**, 429–436 (1999).
2. U. Siegenthaler *et al.*, *Science* **310**, 1313–1317 (2005).
3. D. Lüthi *et al.*, *Nature* **453**, 379–382 (2008).
4. B. Bereiter *et al.*, *Proc. Natl. Acad. Sci. U.S.A.* **109**, 9755–9760 (2012).
5. J. Ahn, E. J. Brook, *Nat. Commun.* **5**, 3723 (2014).
6. S. A. Marcott *et al.*, *Nature* **514**, 616–619 (2014).
7. H. Fischer *et al.*, *Nat. Geosci.* **11**, 474–485 (2018).
8. J. Ahn, E. J. Brook, *Science* **322**, 83–85 (2008).
9. E. Monnin *et al.*, *Science* **291**, 112–114 (2001).
10. J. Jouzel *et al.*, *Science* **317**, 793–796 (2007).
11. T. F. Stocker, S. J. Johnsen, *Paleoceanography* **18**, 1087 (2003).
12. J. Ahn, E. J. Brook, A. Schmittner, K. Kreutz, *Geophys. Res. Lett.* **39**, 5 (2012).
13. T. K. Bauska *et al.*, *Geophys. Res.* **45**, 7731–7740 (2018).
14. S. R. Hemming, *Rev. Geophys.* **42**, RG1005 (2004).
15. L. G. Henry *et al.*, *Science* **353**, 470–474 (2016).
16. Heinrich stadials are directly linked to massive glacial ice and meltwater discharges from the Hudson Strait known as Heinrich events.
17. M. Baumgartner *et al.*, *Clim. Past* **10**, 903–920 (2014).
18. R. H. Rhodes *et al.*, *Science* **348**, 1016–1019 (2015).
19. L. B. Railsback, P. L. Gibbard, M. J. Head, N. R. G. Voarintsoa, S. Toucanne, *Quat. Sci. Rev.* **111**, 94–106 (2015).
20. Materials and methods are available as supplementary materials.
21. L. Loulergue *et al.*, *Nature* **453**, 383–386 (2008).
22. Benthic $\delta^{13}C$ of *C. wuellerstorfi* reflects changes in deep-water ventilation related to reorganization of deep-ocean circulation and remineralization of organic carbon. The $\delta^{18}O$ signal of the same species indicates variations in deep-water temperatures.
23. Millennial-scale changes in the planktic $\delta^{18}O$ record of *G. bulloides* follow changes in the sea surface temperature in the North Atlantic.
24. P. C. Tzedakis *et al.*, *Nat. Geosci.* **2**, 751–755 (2009).
25. P. C. Tzedakis *et al.*, *Clim. Past* **8**, 1473–1485 (2012).
26. T. Rodrigues *et al.*, *Quat. Sci. Rev.* **172**, 118–130 (2017).
27. F. Lambert, M. Bigler, J. P. Steffensen, M. Hutterli, H. Fischer, *Clim. Past* **8**, 609–623 (2012).
28. N. J. Shackleton, M. A. Hall, E. Vincent, *Paleoceanography* **15**, 565–569 (2000).
29. R. Schneider, J. Schmitt, P. Köhler, F. Joos, H. Fischer, *Clim. Past* **9**, 2507–2523 (2013).
30. T. K. Bauska *et al.*, *Proc. Natl. Acad. Sci. U.S.A.* **113**, 3465–3470 (2016).
31. F. Joos, R. Spahni, *Proc. Natl. Acad. Sci. U.S.A.* **105**, 1425–1430 (2008).
32. P. Tans, R. Keeling, Annual mean CO_2 growth rate for Mauna Loa, Hawaii (NOAA/ESRL and Scripps Institution of Oceanography, 2020); www.esrl.noaa.gov/gmd/ccgg/trends/gr.html.
33. T. Extier *et al.*, *Quat. Sci. Rev.* **185**, 244–257 (2018).
34. L. Bazin *et al.*, *Clim. Past* **9**, 1715–1731 (2013).
35. H. Cheng *et al.*, *Nature* **534**, 640–646 (2016).
36. A. Bozbiyik, M. Steinacher, F. Joos, T. F. Stocker, L. Menviel, *Clim. Past* **7**, 319–338 (2011).
37. R. M. Spratt, L. E. Lisiecki, *Clim. Past* **12**, 1079–1092 (2016).
38. S. Barker *et al.*, *Nature* **520**, 333–336 (2015).
39. A. J. Dickson *et al.*, *Nat. Geosci.* **2**, 428–433 (2009).
40. R. G. Hatfield *et al.*, *Earth Planet. Sci. Lett.* **454**, 225–236 (2016).
41. D. J. Wilson *et al.*, *Nature* **561**, 383–386 (2018).
42. J. B. Pedro *et al.*, *Quat. Sci. Rev.* **192**, 27–46 (2018).
43. T. Chen *et al.*, *Science* **349**, 1537–1541 (2015).
44. S. L. Jaccard, E. D. Galbraith, A. Martínez-García, R. F. Anderson, *Nature* **530**, 207–210 (2016).
45. C. Basak *et al.*, *Science* **359**, 900–904 (2018).
46. B. B. Stephens, R. F. Keeling, *Nature* **404**, 171–174 (2000).
47. A. Schmittner, E. D. Galbraith, *Nature* **456**, 373–376 (2008).
48. M. Lacerra, D. Lund, J. Yu, A. Schmittner, *Paleoceanography* **32**, 780–795 (2017).
49. L. Menviel *et al.*, *Nat. Commun.* **9**, 2503 (2018).
50. J. W. B. Rae *et al.*, *Nature* **562**, 569–573 (2018).
51. P. Köhler, G. Knorr, E. Bard, *Nat. Commun.* **5**, 5520 (2014).
52. A. Jeltsch-Thömmes, F. Joos, *Clim. Past* **16**, 423–451 (2020).
53. C. Buizert *et al.*, *Nature* **563**, 681–685 (2018).

54. P. U. Clark *et al*., *Nat. Clim. Chang.* **6**, 360–369 (2016).
55. C. Nehrbass-Ahles *et al*., High-resolution atmospheric CO_2 and CH_4 records derived from the EPICA Dome C ice core and stable isotope records from marine sediment core IODP Site U1385 covering MIS 9e - 12a, PANGAEA (2020); https://doi.org/10.1594/PANGAEA.915146.

ACKNOWLEDGMENTS

We thank M. Häberli, O. Eicher, S. Eggleston, C. Bréant, J. Beck, and B. Seth for assistance with sample acquisition. We acknowledge the support of G. Aufresne, who conducted additional CH_4 measurements at IGE. Samples from site U1385 were provided by the International Ocean Discovery Program (IODP). J. Booth, S. Crowhurst, J. Nicolson, J. Rolfe, and M. Mleneck-Vautravers provided laboratory support. Thanks to R. Walther, S. Marending, K. Grossenbacher, H. P. Moret, and R. Bleisch for technical assistance and E. Brook for helpful comments on an earlier version of the manuscript. **Funding:** This work is a contribution to the European Project for Ice Coring in Antarctica (EPICA), a joint European Science Foundation and European Commission scientific program, funded by the European Union and by national contributions from Belgium, Denmark, France, Germany, Italy, the Netherlands, Norway, Sweden, Switzerland, and the United Kingdom. Main logistic support was provided by IPEV and PNRA. This is EPICA publication no. 315. C.N.-A., J.Sc., B.B., F.J., A.S., L.Sc., L.Si., H.F., and T.F.S. acknowledge long-term financial support from the Swiss National Science Foundation (SNF project numbers 200020_159563, 200020_172745, 200020_172506, 200020_172476, and 20FI21_189533). This project is TiPES (Tipping Points in the Earth System) contribution no. 17. This project has received funding from the European Union's Horizon 2020 research and innovation program under grant 820970 and from the European Community's Seventh Framework Programmes ERC-2011-AdG under grant agreement 291062 (ERC ICE&LASERS). J.Sh. is supported by the LabEX OSUG@2020 project of the Grenoble Observatory of Sciences of the Universe (OSUG). **Author contributions:** C.N.-A., J.Sc., B.B., J.C., D.H., H.F., and T.F.S. designed the research. C.N.-A. performed the measurements with contributions from J.Sh., A.S., G.T., and R.G. Data analyses were led by C.N.-A. with contributions from J.Sc., B.B., F.J., L.Sc., L.Si., D.H., H.F., and T.F.S. C.N.-A. and T.F.S. led the writing of the manuscript, with input from all authors. **Competing interests:** The authors declare no competing interests. **Data and materials availability:** All data are available online in the supplementary materials and through the PANGAEA data depository (*55*).

SUPPLEMENTARY MATERIALS

science.sciencemag.org/content/369/6506/1000/suppl/DC1
Materials and Methods
Supplementary Text
Figs. S1 to S9
Table S1
References (*56*–*87*)
Data S1 and S2

2 August 2019; accepted 9 July 2020
10.1126/science.aay8178

Science

Abrupt CO_2 release to the atmosphere under glacial and early interglacial climate conditions

C. Nehrbass-Ahles, J. Shin, J. Schmitt, B. Bereiter, F. Joos, A. Schilt, L. Schmidely, L. Silva, G. Teste, R. Grilli, J. Chappellaz, D. Hodell, H. Fischer and T. F. Stocker

Science **369** (6506), 1000-1005.
DOI: 10.1126/science.aay8178

Pulses of the past

Bursts of carbon dioxide, released into the atmosphere and occurring on centennial time scales, were seen during the cold periods of the last glacial cycle but not in older or warmer conditions. Nehrbass-Ahles *et al.* present a record of atmospheric carbon dioxide concentrations retrieved from the European Project for Ice Coring in Antarctica Dome C ice core showing that these carbon dioxide jumps occurred during both cold and warm periods between 330,000 and 450,000 years ago. They relate these pulses to disruptions of the Atlantic meridional overturning circulation caused by freshwater discharge from ice sheets. Such rapid carbon dioxide increases could occur in the future if global warming also disrupts this ocean circulation pattern.

Science, this issue p. 1000

Science (print ISSN 0036-8075; online ISSN 1095-9203) is published by the American Association for the Advancement of Science, 1200 New York Avenue NW, Washington, DC 20005. The title *Science* is a registered trademark of AAAS.